# Performance Analysis on an MAP Fine Timing Algorithm in UWB Multiband OFDM

Christian R. Berger, *Student Member, IEEE,* Shengli Zhou, *Member, IEEE,* Zhi Tian, *Senior Member, IEEE,* and Peter Willett, *Fellow, IEEE*

***Abstract*—In this paper we develop a fine synchronization algorithm for multiband OFDM transmission in the presence of frequency selective channels. This algorithm is based on maximum a posteriori (MAP) joint timing and channel estimation that incorporates channel statistical information, leading to considerable performance enhancement relative to existing maximum likelihood (ML) approaches. We carry out a thorough performance analysis of the fine timing algorithm, and link the diversity concept widely used in data communications to the timing performance. We show that the probability of the timing offset equal to or larger than $\Delta$ taps has a diversity order of $N_B \min(\Delta, L)$ in Rayleigh fading channels, where $N_B$ is the number of subbands and $L$ is the number of channel taps. This result reveals that the timing estimate is very much concentrated around the true timing as the signal to noise ratio (SNR) increases. Our simulations confirm the theoretical analysis, and also demonstrate the robustness of the proposed timing algorithm against model mismatches in a realistic UWB indoor channel.**

***Index Terms*—UWB, multiband OFDM, positioning, timing, synchronization, diversity, performance analysis.**

## I. Introduction

POSITIONING in wireless networks is an attractive topic, and its uses range from localization to geo-routing and position-aware applications. Many positioning algorithms utilize time of arrival (TOA) or time difference of arrival (TDOA) measurements, which can be obtained from point-to-point communication links [1]. In this context, high timing accuracy translates into precise ranging information. Ultra Wideband (UWB) signaling promises high time resolution thanks to its inherently large bandwidth. Recently, timing using the impulse radio (IR) UWB waveforms has been actively studied; see e.g., [1] and references therein. We in this paper develop timing algorithms using the multiband OFDM UWB signals [2]. UWB channels exhibit dense multipath. To extract timing information from a communication link, one needs to locate the "first arrival" in the presence of dense multipath. This first path is not necessarily the strongest one due to channel fading [1]. Therefore at high bandwidths, traditional correlation-based timing algorithms are not bandwidth limited, but *multipath* limited — as the estimated timing varies with the realization of which path is the strongest in dense multipath. OFDM signaling has unique capabilities in handling multipath channels, which can be exploited for accurate timing.

Since OFDM modulation has been widely used in recent broadband wireless systems, including digital audio/video broadcasting and wireless local/metropolitan area networks, the literature on OFDM synchronization is thus rich, see e.g., [3]–[9], and references therein. However, for communication purposes, OFDM does not require precise timing. Small or moderate offsets in the time domain translate to phase shifts in the frequency domain, which can be estimated by pilot tones, or bypassed by differential modulation. For this reason, there has been only a few fine timing algorithms for OFDM [5]–[9], where a maximum-likelihood (ML) approach is usually adopted for joint channel and delay estimation.

For synchronization of multiband OFDM, we first rely on the algorithm of [3] for coarse timing to capture data blocks that contains circular convolution between the channels and the OFDM data symbols. We then apply maximum a posteriori (MAP) estimation to derive solutions to joint channel and delay estimation. Relying on analytical tools for non-coherent data detection with diversity combining [10], we carry out a thorough performance analysis for timing in the presence of frequency-selective fading channels. For multiband OFDM on Rayleigh channels with a uniform power decay profile, the probability of the timing estimate being off the true timing by $\Delta$ taps has a diversity order of $N_B \min(\Delta, L)$, where $N_B$ is the number of bands and $L$ is the number of channel taps. This result reveals that the timing estimate is very much concentrated around the true timing as SNR increases. This is not the case for a correlation-based synchronization algorithm that looks for the strongest channel tap of the current channel realization.

Our main distinctions from existing works in [5]–[9] are:

1) Our proposed fine timing algorithm incorporates statistical channel information to considerably improve the timing performance. Such a formulation was not available before.
2) We link the diversity concept well known in data communications to the synchronization performance, which provides valuable insights. Such a link had not been made before.
3) We have considered multiband OFDM, while existing works focus on single band OFDM.

The rest of this paper is as follows. We present the synchronization algorithm in Section II, and carry out a performance

Paper approved by H. Minn, the Editor for Synchronization and Equalization of the IEEE Communications Society. Manuscript received October 28, 2006, revised May 7, 2007 and September 4, 2007. C. R. Berger, S. Zhou, and P. Willett are supported by ONR grant N00014-07-1-0429. S. Zhou is also partially supported by the UConn Research Foundation (UCRF) internal grant 448485. Z. Tian is partially supported by NSF under grant ITR ECS-0427430. This paper was presented in part at the International Conference on Ultra Wideband (ICUWB) in Waltham, MA, Sept. 2006.

C. R. Berger, S. Zhou, and P. Willett are with the Department of Electrical and Computer Engineering, University of Connecticut, 371 Fairfield Way U-2157, Storrs, Connecticut 06269, USA (e-mail: {crberger, shengli, willett}@engr.uconn.edu).

Z. Tian is with the Department of Electrical and Computer Engineering, Michigan Technological University, Houghton, Michigan 49931, USA (e-mail: ztian@mtu.edu).

Digital Object Identifier 10.1109/TCOMM.2008.060592.

analysis in Section III. We present numerical results in Section IV, and conclude in Section V.

## II. Multiband OFDM Synchronization

For mathematical tractability and ease of presentation, we first list the adopted assumptions in deriving the fine synchronization algorithm which is based on joint delay and channel estimation.

A1) The discrete-time[1] frequency selective channel has $L$ taps, contained in $\mathbf{h}_i := [h_{i,0}, \cdots, h_{i,L-1}]^T$ the channel vector in the $i$th band. The number of taps $L$ is known at the receiver.

A2) Channel vectors $\mathbf{h}_1, \ldots, \mathbf{h}_{N_B}$ are uncorrelated over different frequency bands. Each channel vector $\mathbf{h}_i$ is complex Gaussian distributed with zero mean and a diagonal covariance matrix $\mathbf{R}_{\mathbf{h}_i} = \text{diag}(\sigma^2_{h_{i,0}}, \ldots, \sigma^2_{h_{i,L-1}})$.

A3) A coarse synchronization of [3] has been used[2] and the coarse synchronization yields a delay estimate $d \in [-(N_g - L), 0]$, where $N_g$ is the length of the OFDM cyclic prefix. But no knowledge on the distribution of $d$ from the coarse synchronization is available.

A4) Carrier frequency offset (CFO) can be ignored or has been compensated already in the received sequence. (The impact of CFO will be tested by numerical results.)

A5) All entries of the OFDM information symbols are drawn from a signal constellation with unit amplitude, e.g., phase-shift-keying (PSK) modulation.

Multiband OFDM splits the whole UWB spectrum into multiple subbands, and adopts frequency hopped OFDM transmission across the subbands. For example, the multiband OFDM in [2] uses subbands of 528 MHz each, and the hopping is done on an OFDM symbol-by-symbol basis. Let $N_c$ denote the number of subcarriers in OFDM. On the $i$th frequency band, the transmitter converts a data vector of length $N_c$, denoted by $\mathbf{s}_i = [s_{i,0} \cdots s_{i,N_c-1}]^T$, to the corresponding OFDM symbol $\mathbf{x}_i = \mathbf{F}^H \mathbf{s}_i$ via inverse Fourier transform, where $(\cdot)^H$ denotes the Hermitian transpose and $\mathbf{F}$ is the discrete Fourier transform (DFT) matrix of dimension $N_c \times N_c$ with the $(l+1, k+1)$th entry $[\mathbf{F}]_{l,k} = \frac{1}{\sqrt{N_c}} \exp(-j2\pi lk/N_c), l, k = 0, \ldots, N_c - 1$. Cyclic prefixes (CP), which are simply the last $N_g$ samples of the OFDM block, are inserted before each OFDM symbol as a guard interval.

After coarse synchronization, the receiver takes a received vector $\mathbf{y}_i$ of length $N_c$ starting at $d$, as illustrated in Fig. 1. Assumption A2 ensures that the block $\mathbf{y}_i$ contains an *exact* cyclic convolution between the channel vector $\mathbf{h}_i$ and the transmitted symbol block $\mathbf{x}_i$; though the proposed timing algorithm will still work in practice if an exact cyclic convolution is not available due to edge effects. To use a matrix-vector form to

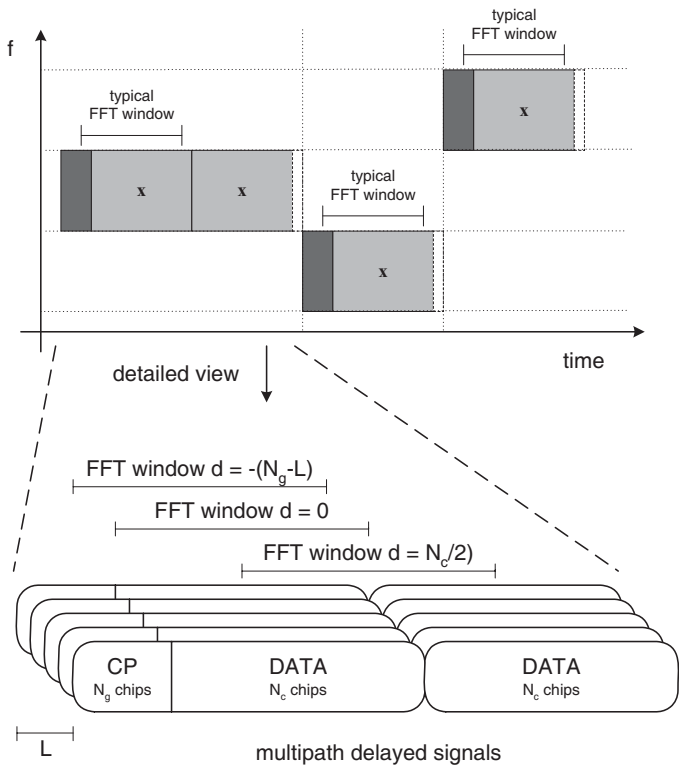


Fig. 1. Transmitted signals for multiband OFDM synchronization and detailed view of coarse synchronization in multipath

represent cyclic convolution, we define an $N_c \times N_c$ circular shift matrix $\mathbf{J}$ and an $N_c \times L$ zero-insertion matrix $\mathbf{T}$ as

$$\mathbf{J} = \begin{bmatrix} \mathbf{0}_{1\times(N_c-1)} & 1 \\ \mathbf{I}_{(N_c-1)} & \mathbf{0}_{(N_c-1)\times 1} \end{bmatrix}, \quad \mathbf{T} = \begin{bmatrix} \mathbf{I}_L \\ \mathbf{0}_{(N_c-L)\times L} \end{bmatrix}.$$

The matrix $\mathbf{J}^k$ will perform a circular shift on a vector by $k$ entries. $\mathbf{J}^k$ is well defined for both $k > 0$ (right shift) and $k < 0$ (left shift). Define a circulant matrix

$$\mathbf{X}_i = [\mathbf{x}_i, \mathbf{J}\mathbf{x}_i, \ldots, \mathbf{J}^{N_c-1}\mathbf{x}_i]. \tag{1}$$

With assumptions A1-A3, we have

$$\mathbf{y}_i = \mathbf{X}_i \mathbf{J}^d \mathbf{T} \mathbf{h}_i + \mathbf{w}_i, \tag{2}$$

where $\mathbf{w}_i$ contains the additive white Gaussian noise (AWGN) with variance $N_0$.

The joint PDF of all $\mathbf{y}_i, \mathbf{h}_i$ and $d$ is

$$p(\mathbf{y}_1, \ldots, \mathbf{y}_{N_B}, \mathbf{h}_1, \ldots, \mathbf{h}_{N_B}, d) = p(d) \prod_{i=1}^{N_B} p(\mathbf{y}_i, \mathbf{h}_i \mid d). \tag{3}$$

The joint MAP estimates of all $\mathbf{h}_i$ and $d$ are determined through

$$\left\{ \{\hat{\mathbf{h}}_i\}_{i=1}^{N_B}, \hat{d} \right\}_{\text{MAP}} = \arg\max_{\mathbf{h}_i, d} p(d) \prod_{i=1}^{N_B} p(\mathbf{y}_i, \mathbf{h}_i \mid d). \tag{4}$$

We will use a search interval of $(-N_c/2, N_c/2]$ on $d$ assuming[3] that $p(d) = 1/N_c$. Due to the Gaussian assumptions on

[1]Note that we just estimate the delay as multiples of the sampling period, and absorb the effects of fractional delay and filter effects into the channel coefficients; see a discussion in e.g., [7]. The number of channel taps could be known a priori relying on channel models, or jointly estimated with the channel itself, as in [5].

[2]The coarse synchronization algorithm of [3] uses two identical OFDM symbols with one cyclic prefix, as shown in the first frequency band in Fig. 1. The delay estimate of [3] is expected to be centered around $-(N_g - L)/2$; see also Fig. 2(a).

[3]Note that the distribution on $d$ may not be uniform and may be correlated with the channel realizations. We choose to neglect possible prior information on $d$, as this will make our algorithm independent of a particular implementation of the coarse synchronization algorithm, and considerably simplify the analysis. However, our simulations in Section IV will test practical scenarios where both of these assumptions could be violated.

$\mathbf{h}_i$ and $\mathbf{w}_i$, we have

$$\left\{\{\hat{\mathbf{h}}_i\}_{i=1}^{N_B}, \hat{d}\right\}_{\text{MAP}} = \arg\min_{\mathbf{h}_i, d} \sum_{i=1}^{N_B} \left[\frac{1}{N_0}||\mathbf{y}_i - \mathbf{X}_i\mathbf{J}^d\mathbf{T}\mathbf{h}_i||^2 + \mathbf{h}_i^H\mathbf{R}_{\mathbf{h}_i}^{-1}\mathbf{h}_i\right], \quad (5)$$

after straightforward derivations. For each tentative value of $d$, the MAP channel estimate is

$$\hat{\mathbf{h}}_{i,\text{MAP}}(d) = E[\mathbf{h}_i|\mathbf{y}_i, d] = \frac{1}{N_c}\mathbf{D}_i\mathbf{T}^H\mathbf{J}^{-d}\mathbf{X}_i^H\mathbf{y}_i, \quad (6)$$

where $\mathbf{D}_i$ is a $L \times L$ diagonal matrix with the $k$th diagonal entry as $\sigma_{h_{i,k}}^2 / \left(\sigma_{h_{i,k}}^2 + N_0/N_c\right)$; the fact of $\mathbf{X}_i^H\mathbf{X}_i = N_c\mathbf{I}_{N_c}$ is used in the derivation due to assumption A5. Substituting $\hat{\mathbf{h}}_{i,\text{MAP}}(d)$ into the cost function in (5), we find the MAP estimate of $d$ as:

$$\hat{d} = \arg\max_{d} \sum_{i=1}^{N_B} \left|\left| \frac{1}{N_c}\mathbf{D}_i^{\frac{1}{2}}\mathbf{T}^H\mathbf{J}^{-d}\mathbf{X}_i^H\mathbf{y}_i \right|\right|^2. \quad (7)$$

Define a tentative channel estimate as

$$\tilde{\mathbf{h}}_i = \frac{1}{N_c}\mathbf{X}_i^H\mathbf{y}_i = \frac{1}{\sqrt{N_c}}\mathbf{F}^H\text{diag}\{\mathbf{s}_i^H\}\mathbf{F}\mathbf{y}_i. \quad (8)$$

The MAP estimator in (7) simplifies to

$$\hat{d} = \arg\max_{d} \sum_{i=1}^{N_B}\sum_{k=0}^{L-1} \left(\frac{\sigma_{h_{i,k}}^2}{\sigma_{h_{i,k}}^2 + N_0/N_c}\right) |\tilde{h}_{i,[k+d]}|^2, \quad (9)$$

where the subscript $[k+d]$ stands for $(k+d) \mod N_c$. The MAP estimator in (9) combines the channel energy from all branches to decide on the best estimate of $d$.

**Remark 1** In the special case of no knowledge on the distribution of the channel taps, $\mathbf{R}_{\mathbf{h}_i}$ is assumed to be proportional to an identity matrix. (7) simplifies to

$$\hat{d} = \arg\max_{d} \sum_{i=1}^{N_B}\sum_{k=0}^{L-1} |\tilde{h}_{i,[k+d]}|^2, \quad (10)$$

corresponding to a rectangular sliding window. This rectangular sliding window has been used in [5]–[7], [9], starting from an ML approach for the case of $N_B = 1$. Our MAP approach incorporates the prior channel statistical information for performance improvement on the delay estimation.

## III. Timing Performance Analysis

We now analyze the performance of the proposed fine timing algorithm. First, let us take a closer look at the tentative channel estimate $\tilde{\mathbf{h}}$ in (8), on which we operate a sliding window correlator to determine the fine timing, c.f, (9). Substituting (2) into (8), we have:

$$\tilde{\mathbf{h}}_i = \frac{1}{N_c}\mathbf{X}_i^H\left(\mathbf{X}_i\mathbf{J}^d\mathbf{T}\mathbf{h}_i + \mathbf{w}_i\right) = \mathbf{J}^d\mathbf{T}\mathbf{h}_i + \tilde{\mathbf{w}}_i, \quad (11)$$

where the noise vector $\tilde{\mathbf{w}}_i$ remains white but with variance $N_0/N_c$.

This is a problem of signal detection in the presence of Gaussian noise: we have to decide at which sample $\hat{d}$, out of the $N_c$ possibilities, a waveform of length $L$ starts. For $L = 1$ the problem formulation is equivalent to non-coherent detection of orthogonal FSK on a fading channel, for $L \neq 1$ the problem changes to non-orthogonal FSK. Due to the random phase of the signal, the MAP derivation naturally led to a type of energy detector [10].

The pair-wise error probability (PEP) of that the timing metric at $\hat{d} = d + \nu$ is larger than the counterpart at the true timing $d$ can be expressed as:

$$\text{PEP}(\nu) = \Pr\left\{\sum_{i=1}^{N_B}\sum_{k=0}^{L-1} c_{i,k}|\tilde{h}_{i,[k+d]}|^2 < \sum_{i=1}^{N_B}\sum_{k=0}^{L-1} c_{i,k}|\tilde{h}_{i,[k+d+\nu]}|^2\right\} \quad (12)$$

using the weights $c_{i,k} = \sigma_{h_{i,k}}^2/(\sigma_{h_{i,k}}^2 + N_0/N_c)$. Once the PEP is found, we can apply the union bound to assess the timing performance. For purpose of ranging, it is important to achieve a small mean-square-error (MSE) $E\{|d - \hat{d}|^2\}$ — but since we link this formulation to a detection problem, we are interested in the probability of a timing offset larger than or equal to a constant $\Delta$:

$$\Pr(|\hat{d} - d| \geq \Delta) \leq \sum_{\nu=-N_c/2;\ |\nu|\geq\Delta}^{N_c/2} \text{PEP}(\nu). \quad (13)$$

We term the probability to miss the true timing ($\Delta = 0$) as the mis-timing event. We next specify how to evaluate the PEP($\nu$).

### A. The General Case

To derive the PEP with an arbitrary sliding window and Gaussian channel taps from an arbitrary power decay profile, we rewrite the argument of (12) as

$$\Lambda(\nu) = \sum_{i=1}^{N_B}\sum_{k=0}^{L-1+\nu} (c_{i,k} - c_{i,k-\nu})\,|\tilde{h}_{i,[k+d]}|^2 = \sum_{j=0}^{N_B(L-1+\nu)} y_j \quad (14)$$

where the $c_{i,k} = 0$ for $k \notin [1, L]$. Accordingly $y_j$ is generalized exponential with

$$f_Y(y_j) = \frac{1}{|\lambda_j|}e^{-\frac{y_j}{\lambda_j}}U(\lambda_j y_j), \quad (15a)$$

$$\lambda_{k+(i-1)N_B} = (c_{i,k} - c_{i,k-\nu})E\left[|\tilde{h}_{i,[k+d]}|^2\right], \quad (15b)$$

where $U(x)$ is the unit step function. Note that the parameter $\lambda_j$ can be negative, implying that the random variable could be exponentially distributed on the negative half of the $x$-axis. Using that the PDF of a sum of independent random variables is the convolution of the individual PDF's, the characteristic function is the product of the individual characteristic functions

$$F_\Lambda(s) = \prod_{j=0}^{N_B(L-1+\nu)} (1 - j2\pi s\lambda_j)^{-1} = \sum_{j=0}^{N_B(L-1+\nu)} \frac{r_j}{(1 - j2\pi s\lambda_j)^{p_j}}. \quad (16)$$

The $p_j$'s in (16) are introduced to account for possible second order poles when $\lambda_j = \lambda_i, j \neq i$, while the $r_j$'s are found via partial fraction decomposition. The terms in the summation in (16) are characteristic functions of Chi-square random variables of order $2p_j$, therefore the Fourier transform of $F_\Lambda(s)$ will be a sum of different Chi-square PDF's with coefficients $r_j$. The probability that $\Lambda(\nu) \leq 0$ can be determined easily, since the Chi-square PDF's in (16) are only non-zero for $x \leq 0$ if $\lambda_j < 0$. Therefore the PEP comes out to the sum of the $r_j$'s associated with negative $\lambda_j$'s. Thus, the PEP in (12) is

$$\text{PEP}(\nu) = \int_{-\infty}^{0} f_\Lambda(x)\, dx = \sum_{j=0}^{N_B(L-1+\nu)} r_j U(-\lambda_j). \quad (17)$$

### B. The Special Case With Uniform Window

In this section, we take a close look at the special case with uniform window where all $c_{i,k}$'s are the same. This happens in two scenarios i) the SNR is sufficiently high, i.e., $N_0 \to 0$. This is applicable to channels with non-uniform delay profiles; ii) The channel taps have equal energy $\sigma^2_{h_{i,k}} = 1/L$. In this case, the sliding window is uniform at any SNR.

Assuming uniform weights, for $1 \leq \nu \leq L$ common terms in (12) cancel out and we obtain

$$\text{PEP}(\nu) = \Pr\left\{ \sum_{k=0}^{\nu-1} \sum_{i=1}^{N_B} |\tilde{h}_{i,[k+d]}|^2 < \sum_{k=L}^{L+\nu-1} \sum_{i=1}^{N_B} |\tilde{h}_{i,[k+d]}|^2 \right\} \quad (18)$$

This is the error probability of non-coherent detection with receiver diversity combining over $\nu N_B$ branches [10, chapter 14.4], where the right hand side contains all noise with equal power leading to a chi-square distribution, and the left hand side is the sum of the different diversity branches.

We next explore the case where all channel taps have the same variance. The left side of (18) turns to a chi-square distribution with higher variance. We can directly use the result from [10, eq. (14.4-15)]: Assuming uniform power decay profile on each subband $\sigma^2_{h_{i,k}} = 1/L$, the pair-wise error probability events can be calculated as

$$\text{PEP}(\nu) = \frac{1}{(2 + N_c\bar{\gamma}/L)^{\nu N_B}} \times \sum_{k=0}^{\nu N_B - 1} \binom{\nu N_B - 1 + k}{k} \left( \frac{1 + N_c\bar{\gamma}/L}{2 + N_c\bar{\gamma}/L} \right)^k, \quad (19)$$

for $1 \leq \nu \leq L$. At high SNR $\bar{\gamma} \gg 1$, we simplify (19) as [10, eq. (14.4-18)]:

$$\text{PEP}(\nu) \approx \binom{2\nu N_B - 1}{\nu N_B} \left( \frac{N_c}{L}\bar{\gamma} \right)^{-\nu N_B}, 1 \leq \nu \leq L. \quad (20)$$

Therefore, PEP($\nu$) has diversity order $\nu N_B$ for $|\nu| \leq L$; i.e., when plotting PEP($\nu$) versus SNR on a log-log scale, this curve becomes a straight line with slope $-\nu N_B$. Diversity order is one important performance indicator, as it specifies how fast the performance improves as SNR increases.

Since the sliding window is of length $L$, we infer that

$$\text{PEP}(\nu) = \text{PEP}(L), \quad L < \nu < N_c/2. \quad (21)$$

We can derive PEP in a similar fashion when $\nu$ is negative, since all channel taps are i.i.d., thus

$$\text{PEP}(\nu) = \text{PEP}(|\nu|), \quad \nu < 0. \quad (22)$$

Substituting the PEP($\nu$) of (19) into the union bound in (13), we see that low diversity events will dominate at high SNR. In summary, we have the following conclusion.

**Proposition 1** *Under assumptions A1-A5 and when all channel taps have the same variance $\sigma^2_{h_{i,k}} = 1/L$, the probability of timing offset equal to or larger than $\Delta$ is upper bounded by*

$$\Pr(|\hat{d} - d| \geq \Delta) \leq \begin{cases} 2\sum_{\nu=\Delta}^{L} \text{PEP}(\nu) + (N_c - 2L)\text{PEP}(L), & \text{for } \Delta \leq L \\ (N_c - 2\Delta)\text{PEP}(L), & \text{otherwise} \end{cases} \quad (23)$$

*where the closed-form expression for* PEP($\nu$) *is given in* (19)*. At high SNR, the probability of timing offset equal to or larger than $\Delta$ has diversity order $N_B \min(\Delta, L)$.*

To our knowledge, this is the first time the diversity concept widely used in data communications is linked to synchronization performance. This link provides valuable insight. It reveals that the timing estimate of the proposed algorithm is very much concentrated around the true timing when the SNR increases. On the contrary, consider a correlation-based synchronization algorithm in the presence of a channel with uniform power profile, which is the worst-case for synchronization. All channel taps are equally likely to be the strongest one, thus the timing estimate more or less spreads uniformly across the whole channel duration. One cannot improve its performance by improving the timing resolution or increasing the SNR[4].

## IV. Numerical Results

The system parameters are $N_c = 128$, $N_g = 32$, as in [2]. Unless stated otherwise, the channel length is set to $L = 16$, and the channel taps are i.i.d. Rayleigh distributed. Most Monte Carlo simulations use $10^6$ runs and we do not consider CFO unless specified otherwise.

*Case 1: Single Band OFDM ($N_B = 1$).* Fig. 2(a) shows the distribution of the timing delay after coarse synchronization for different levels of SNR, while Fig. 2(b) depicts the counterparts after fine timing. In Fig. 2(a) we can see that assumption A3 is not necessarily true for low SNR, as the coarse timing has some non-negligible probability of being outside $[-16, 0]$. However, when examining Fig. 2(b) we still see a significant improvement in the delay distribution. Thus, even if the coarse synchronization is not as precise as required by assumption A3, the fine timing algorithm still shows an

[4]A similar timing performance analysis for frequency selective channels is available in [7]. The distinctions of our analysis are: i) Our PEP analysis is *exact*, which is linked to *non-coherent* data detection in fading channels. The PEP analysis in [7] is *approximate*, as it drops the squared noise term to make the test variable Gaussian distributed when conditioned on the channel; see the paragraph after eq. (A4). The analysis in [7] is then linked to *coherent* data detection in fading channels. ii) We consider a general sliding window while [7] only uses a rectangular sliding window. iii) The diversity concept was not linked to timing performance in [7].

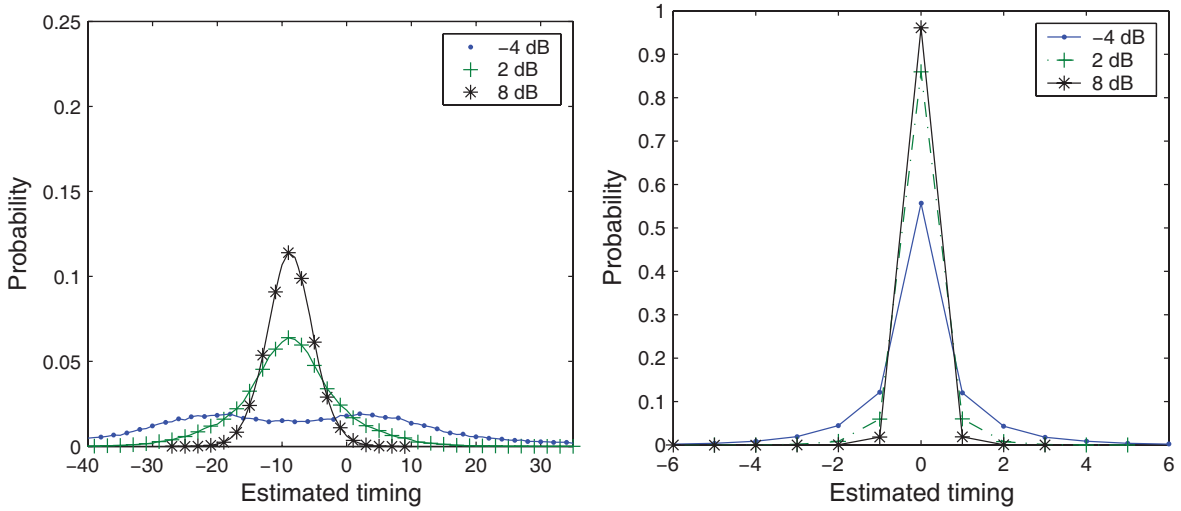


(a) after coarse synchronization

(b) after fine synchronization

Fig. 2. Comparison of timing distribution after coarse acquisition and fine synchronization for $N_B = 1$.

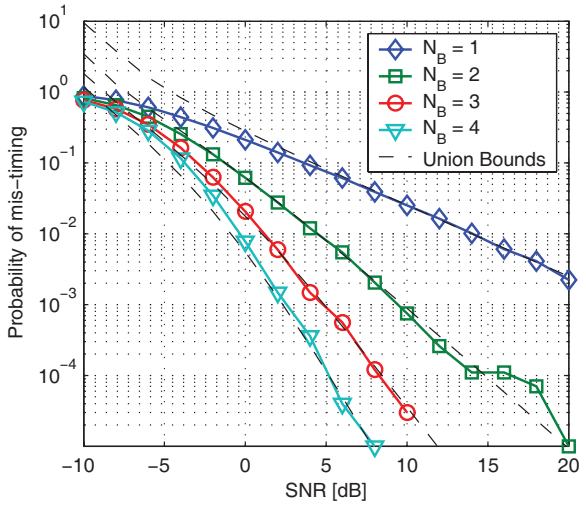


Fig. 3. Probability of mis-timing for multiband OFDM synchronization

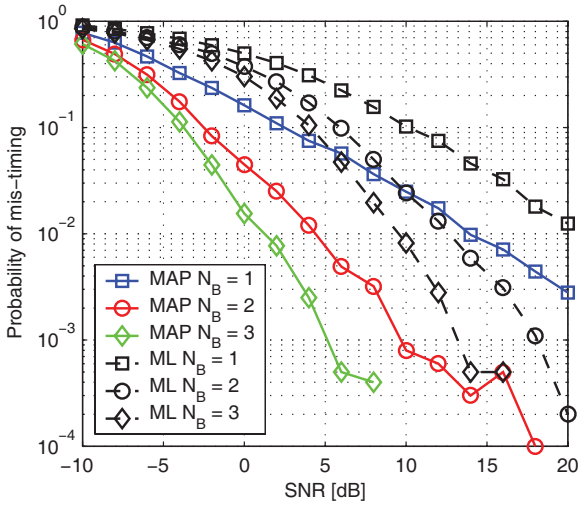


Fig. 4. Comparison between the MAP and ML timing algorithms on a channel with exponential delay profile

acceptable performance. For higher SNR's, the coarse synchronization is very contained in the interval $[-16, 0]$ and the fine synchronization has only noticeable probabilities around $d = 0$. It shows that most estimates concentrate around the correct timing.

*Case 2: Multiband OFDM.* The multiband simulation uses two identical symbols on one frequency band for coarse synchronization and only one symbol on each other frequency band. After diversity combining, the probability of mis-timing decreases with diversity $N_B$ and converges well against the theoretical union bounds (see Fig. 3). It is true that multiband reception also increases the average SNR, however, the slope change of the performance curves has to be attributed to the diversity effect.

*Case 3: MAP versus ML Timing Performance.* We now compare the MAP and ML timing algorithms to see how much statistical channel information can help on the timing performance. We consider a channel of length $L = 16$, with exponentially decreasing profile on each frequency band as: $\sigma^2_{h_k} = 10^{-a}\sigma^2_{h_{k-1}}$. The decay factor $a = 0.1$ leads to a 15 dB difference between the power of the first and last channel taps. With the optimal sliding window for MAP and the uniform window for ML, Fig. 4 demonstrates considerable performance improvement of the MAP algorithm relative to the ML counterpart. Note that the ML algorithm performs poorly at low SNR. This is reasonable, since weak channel taps towards the tail can be easily exchanged for noise samples in the front of the channel without changing much the energy within the uniform sliding window.

*Case 4: Carrier Frequency Offset.* We study the impact of CFO on the timing performance. The CFO is randomly generated within an interval of $[-\epsilon_{\max}, \epsilon_{\max}]$. We choose $\epsilon_{\max} = 10^{-3}$, that corresponds to a CFO of 528kHz in the OFDM UWB setting of [2]. This easily includes any Doppler spreads and oscillator mismatches. For example, a moving speed of 3 m/s with a carrier frequency of 10 GHz would only lead to $\epsilon_{\max} \approx 10^{-6}$; a 40 ppm mismatch between the oscillators at the transmitter and the receiver would lead to $\epsilon_{\max} \approx 6 \cdot 10^{-4}$ at 8 GHz.

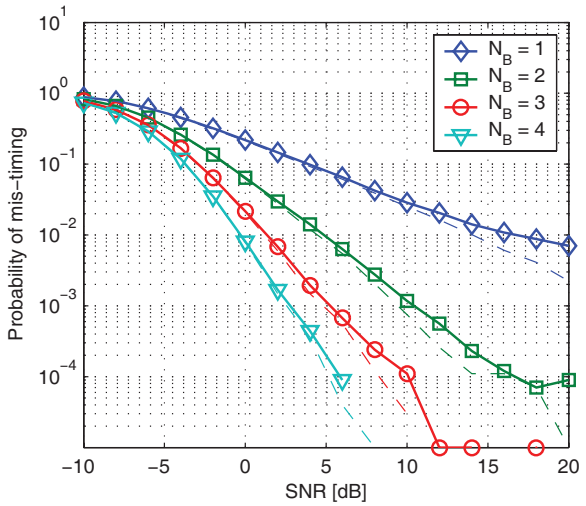


Fig. 5. Comparison of Multiband OFDM synchronization with CFO (full lines) vs. no CFO (dashed lines); $\epsilon \in [-10^{-3}, 10^{-3}]$

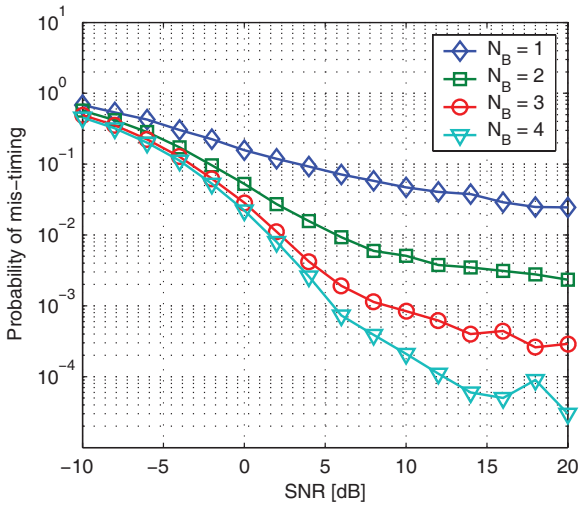


Fig. 6. Multiband OFDM synchronization using a UWB indoor channel

In general, the performance degradation due to small CFOs is barely noticeable at SNR's of interest, as shown in Fig. 5. We argue that for these levels of CFOs, the impact on fine timing is quite negligible and the CFO can be compensated for data demodulation after the synchronization.

*Case 5: UWB Indoor Channel.* We now simulate the timing performance using UWB channels generated from the indoor channel model [12]. This channel model was adopted by the IEEE 802.15.3a standardization task group (TG3a); we use the parameters from channel model (CM) 1 [12]. Since the UWB indoor channel model returns real (non-complex) delayed paths arriving in clusters in continuous time, we have to assign a complex phase, filter and down sample the channel; see e.g., [13] for an equivalent base-band model. As statistical information about the channel, we use the average power decay profile, generating 100 channel tap realizations and averaging their energy.

Fig. 6 depicts the timing performance for multiband OFDM. Compared with the $L$-tap i.i.d. Rayleigh fading channels, the timing performance with the realistic indoor channels demonstrates some performance degradation. This can be attributed to two effects: i) the channel taps not being complex Gaussian distributed, and ii) the UWB indoor channel model yields an almost arbitrarily long channel that eventually vanishes underneath the noise, hence for increasing SNR the channel becomes longer – too long for the CP included in the system design – generating intersymbol interference. Nevertheless, the important messages here are: i) frequency hopping across multiple subbands enhances the diversity order of the timing performance, and ii) the proposed MAP timing algorithm could be robust against mismatches on the needed statistical knowledge, e.g., the distribution and channel length mismatches as illustrated in this example.

## V. Conclusion

We developed a fine timing algorithm for multiband OFDM based on MAP joint channel and delay estimation that incorporates statistical channel information. We analyzed the timing performance, relying on tools from non-coherent data communication in frequency-selective channels. We showed that most timing estimates lie closely around the right timing, with the probability of timing offset equal to or greater than $\Delta$ having diversity order of $N_B \min(\Delta, L)$, where $L$ the number of channel taps and $N_B$ is the number of subbands. We tested the proposed timing algorithm with both Rayleigh and UWB indoor channels.

## References

[1] S. Gezici, Z. Tian, G. B. Giannakis, H. Kobayashi, A. Molisch, V. Poor, and Z. Sahinoglu, "Localization via ultra-wideband radios - a look at positioning aspects of future sensor networks," *IEEE Signal Processing Mag.*, vol. 22, no. 4, pp. 70–84, July 2005.

[2] A. Batra, J. Balakishnan, G. R. Aiello, J. R. Foerster, and A. Dabak, "Design of a multiband OFDM system for realistic UWB channel environments," *IEEE Trans. Microwave Theory and Techniques*, pp. 2123–2138, Sept. 2004.

[3] T. M. Schmidl and D. C. Cox, "Robust frequency and timing synchronization for OFDM," *IEEE Trans. Commun.*, pp. 1613–1621, Dec. 1997.

[4] J. J. van de Beek, M. Sandell, and P. O. Borjesson, "ML estimation of time and frequency offset in OFDM systems," *IEEE Trans. Signal Processing*, pp. 1800–18 005, July 1997.

[5] E. G. Larsson, G. Liu, J. Li, and G. B. Giannakis, "Joint symbol timing and channel estimation for OFDM based WLANs," *IEEE Commun. Lett.*, vol. 5, no. 8, pp. 325–327, Aug. 2001.

[6] H. Minn, V. Bhargava, and K. Letaief, "A robust timing and frequency synchronization for OFDM systems," *IEEE Trans. Wireless Commun.*, pp. 822–839, July 2003.

[7] M. Morelli, "Timing and frequency synchronization for the uplink of an OFDMA system," *IEEE Trans. Commun.*, pp. 296–306, Feb. 2004.

[8] W. C. Lim, B. Kannan, and T. T. Tjhung, "Joint channel estimation and OFDM synchronisation in multipath fading," in *Proc. International Conference on Communications*, 2004, pp. 983–987.

[9] H. Minn, V. Bhargava, and K. Letaief, "A combined timing and frequency synchronization and channel estimation for OFDM," *IEEE Trans. Commun.*, vol. 54, no. 3, pp. 1081–1096, June 2006.

[10] J. G. Proakis, *Digital Communications*, 4th ed. New York: McGraw-Hill, 2001.

[11] M. Morelli and U. Mengali, "Carrier-frequency estimation for transmissions over selective channels," *IEEE Trans. Commun.*, vol. 48, no. 9, pp. 1580–1589, Sept. 2000.

[12] A. F. Molisch, J. R. Foerster, and M. Pendergrass, "Channel models for ultrawideband personal area networks," *IEEE Wireless Commun.*, vol. 10, no. 6, pp. 1247–1257, Aug. 2002.

[13] Y. Li, T. Jacobs, and H. Minn, "Frequency offset estimation for MB-OFDM-based UWB systems," in *Proc. Intl. Conf. on Commun.*, June 2006.